Responsivity and detectivity modelling of thermal radiation sensors based on a biased thermocouple

Ulrich Dillner, Ernst Kessler, Hans-Georg Meyer

Responsivity and detectivity modeling of thermal radiation sensors based on a biased thermocouple

Ulrich Dillner, Ernst Kessler and Hans-Georg Meyer
Institute of Photonic Technology, Albert-Einstein-Str. 9, 07745 Jena, Germany

E-mail: ulrich.dillner@ipht-jena.de

Abstract. Thermal radiation sensors are based on two signal transduction stages: radiation to thermal and thermal to electrical. The most common of these sensors are the radiation thermocouple using the Seebeck effect and the bolometer applying the thermoresistive effect. While the bolometer requires a bias current for signal generation the thermocouple is generally operated unbiased. The paper theoretically investigates a biased thermocouple instead, which can be thought of as a combination of both thermal radiation sensor types. Its responsivity and detectivity is calculated based on previous theories of the performance of bolometers and radiation thermocouples, respectively, thereby including the Peltier effect. The electrical resistance and thermal conductance of the thermocouple as input parameters for these calculations are modeled using a simple strip geometry to facilitate one-dimensional analytical electrothermal modeling.

1. Introduction

Generally, a thermal sensor yields an electrical output signal with an input or intermediate signal of the thermal type [1]. In a thermal radiation sensor, the input signal is the radiation power, which is converted into heat by an absorber. Thus, it creates or changes a temperature gradient in a thermal isolation structure, which constitutes the intermediate signal and is transduced into an electrical output signal by a temperature (difference) sensor. Thermal radiation sensors are advantageous compared to photonic detectors because of their broadband response over the infrared spectrum enabled by appropriate volume absorbers and their uncooled operation due to the thermal sensor principle. Moreover, in the far-infrared or Terahertz range, respectively, input signal reception by antenna-coupling is an option for thermal radiation sensors. The most common thermal radiation sensors are the radiation thermocouple (or thermopile terming a serial connection of thermocouples) and the bolometer. The former uses the thermoelectric or Seebeck effect in a thermocouple to implement a temperature difference sensor while the latter applies the thermoresistive effect, i.e. the temperature dependence of an electric resistor, for temperature sensing. The thermometric transduction coefficient ζ (unit of measurement V/K) indicates the efficiency of the transduction from the thermal to the electrical domain by the temperature sensor. Considering the radiation thermocouple, which generates a thermoelectric signal voltage from the temperature difference between the hot and the cold thermocouple junctions, the transduction coefficient is equal to its Seebeck coefficient γ. In the case of the bolometer, which, contrary to the thermocouple, needs a bias current causing a voltage drop U_{BO} for the generation of the signal voltage, the coefficient is given by the product $\zeta=\alpha_{BO}U_{BO}$. Here $\alpha_{BO}=(1/R_{BO})(dR_{BO}/dT)$ is the temperature coefficient of the bolometer electrical resistance R_{BO}.

The voltage responsivity S_U of a thermal radiation sensor is given by $S_U=\varepsilon\zeta/A$ (ε: absorptivity or emissivity, respectively, A: thermal admittance of the thermal isolation structure). Consequently, each of the two transduction stages of a thermal radiation sensor (radiation to thermal represented by ε and thermal to electrical represented by ζ) should be as efficient as possible while its thermal isolation structure should have the lowest possible admittance. An advantage of the bolometer compared to the radiation thermocouple is the option to raise ζ and, consequently, its responsivity not only by improving the corresponding material property but by increasing the bias current. On the contrary, a bias current implies a more expensive circuitry and an additional source of noise, known as flicker $1/f$ noise.

The purpose of this paper is to investigate theoretically a combination of both thermal radiation sensor types by considering a biased thermocouple. The concept to improve the sensitivity of thermocouples by adapting the principle of the bolometer was proposed as early as 1945 by Conn [2], but pursued hardly ever up to the present. Conn coined the term thermocouple bolometer to designate a biased radiation thermocouple operated like a bolometer. In the following, the responsivity and detectivity of a thermocouple bolometer (TB) will be calculated based on the theories of the performance of bolometers by Jones [3], Smith et al. [4] and Mather [5] and of radiation thermocouples by Smith et al. [4] thereby including the Peltier effect. The electrical resistance and thermal conductance of the TB, which are input parameters for these calculations, will be modeled using a simple strip geometry to facilitate one-dimensional analytical electrothermal modeling. The modeling results will be compared with a conventional resistance bolometer (RB) to assess if thermocouple bolometers can be advantageous in appropriate modes of operation.

2. Power balance equation and bias current

The bias circuit of the thermocouple bolometer is shown in Fig. 1. The bias current I is positive if flowing from p to n through the thermocouple p-n junction as presented in Fig. 1. It causes a proportional Peltier heat flow

$$P_P(T) = \gamma T I\ , \quad \gamma = \gamma_{\mathrm{p}} - \gamma_{\mathrm{n}} \geq 0 \tag{1}$$

(γ_m with m=n, p is the absolute Seebeck coefficient of the m-strip). A negative Peltier heat flow caused by a negative bias current flowing from n to p is related to Peltier cooling. To determine the power input Π to the TB strip the Peltier heat flow has to be added to the Joule heating power P and the radiation induced component W of the power input to the TB, $\Pi=P_P+P+W$. Introducing the total non-radiation induced (i.e., bias induced) heat load $P_T=P_P+P$ generated in a TB strip yields $\Pi=P_T+W$. The power balance equation states that Π is equal to the sum of the power flow to the heat sink P_{th} and the power stored into the thermal capacitance C of the TB strip:

$$\Pi = P_{th} + C\frac{dT}{dt} \tag{2}$$

(t: time). In a small signal analysis, i.e. assuming $T-T_S=\Delta T<<T$ where T and T_S denote the strip average and the heat sink temperatures, respectively, the power flow to the heat sink is proportional to the temperature difference with the thermal conductance G as the proportionality factor, $P_{th}=G\Delta T$, hence

$$\Pi = G\cdot\Delta T + C\cdot\frac{d}{dt}\Delta T\ . \tag{3}$$

Using Fourier transforms Eq. (3) is transformed into the algebraic equation

$$G\cdot\Delta T(\omega) + i\omega C\cdot\Delta T(\omega) = \Pi(\omega) \tag{4}$$

(ω: angular frequency) resulting in

$$\Delta T(\omega) = \frac{\Pi(\omega)}{A(\omega)}\ . \tag{5}$$

Here the definition of the complex thermal admittance

$$A(\omega) = G + i\omega C = G(1+i\omega\tau)\ , \quad \tau = \frac{C}{G} \tag{6}$$

has been employed (τ: thermal time constant). In the DC limit equivalent to ω=0 the complex thermal admittance reduces to the thermal conductance $G=A(0)=A_0$ (as a convention, the index "0" will be used throughout this paper to designate the DC value of a variable).

The temperature difference ΔT, cf. Eq. (5), causes a thermoelectric voltage

$$U_{TE} = \gamma\cdot\Delta T \tag{7}$$

in the TB. U_{TE} corresponds to a thermoelectric impedance $Z_{TE}=U_{TE}/I$ and results in modifications of the expressions concerning the resistance, the voltage drop and the Joule heating power of a TB compared

with a RB as summarized in Table 1. Note that the addition of the thermoelectric impedance due to the Peltier effect is the only modification of the bolometer resistance considered here, which means that additional p-n junction contact effects are assumed to be negligible. While this approach is reasonable for metals or semimetals as materials of the thermocouple, it generally cannot be applied to semiconductors and does not, e.g., include the nonlinear rectifying contact phenomena inherent to a Si p-n junction diode.

For the calculation of the bias current, we consider the limit of negligible radiation power, i.e. $\Delta T=P_T/A$. Now the thermoelectric voltage $U_{TE}=(P_P+P)\gamma/A$ can be expressed in terms of the thermocouple's complex dynamic impedance Z_D defined in [4],

$$U_{TE} = Z_D I + \frac{\gamma}{A} P\,, \quad Z_D = \frac{\gamma^2 T}{A} \geq 0\,. \tag{8}$$

Z_D can be employed to introduce the thermocouple effective resistance R_{TC} by

$$R_{TC} = R_{BO} + Z_D\,. \tag{9}$$

Using Eqs. (8) and (9) the TB resistance $R=R_{BO}+U_{TE}/I$ is rewritten as

$$R = \frac{R_{TC}}{1-Y}\,, \quad Y = \frac{\gamma}{A} I\,. \tag{10}$$

The bias current can be calculated applying Kirchhoff's loop rule to the bias circuit shown in Fig. 1. Adding up the voltage drops $U=U_{BO}+U_{TE}$ across the TB and $U_L=Z_L I$ across the load impedance yields $U_B= U_{BO}+U_{TE}+U_L$. With $U_{BO}=R_{BO}I$ we get

$$I = \frac{U_B - U_{TE}}{R_{BO} + Z_L}\,. \tag{11}$$

Again applying Eqs. (8) and (9) results in

$$I = \frac{U_B - \frac{\gamma P}{A}}{R_{TC} + Z_L}\,. \tag{12}$$

In the further calculations the derivative dI/dT will be required. Differentiation of Eq. (12) yields the equation $(R_{TC}+Z_L)dI+I\cdot dR_{TC}=(-\gamma/A)dP$ assuming that dA is negligible. Using the definition of the temperature coefficient of the thermocouple effective resistance,

$$\alpha_{TC} = \frac{1}{R_{TC}} \frac{dR_{TC}}{dT}\,, \tag{13}$$

and the relation $dP=AdT$ yields $(R_{TC}+Z_L)dI+(I\alpha_{TC}R_{TC}+\gamma)dT=0$, hence,

$$\frac{dI}{dT} = -\frac{I\alpha_{TC}R_{TC} + \gamma}{R_{TC} + Z_L}\,. \tag{14}$$

3. Responsivity of the thermocouple bolometer

The current responsivity is defined by

$$S_I = \frac{dI}{dW} \tag{15}$$

while the voltage responsivity is given by

$$S_U = \frac{dU}{dW}\,. \tag{16}$$

These responsivities are related by

$$\frac{S_U}{S_I} = \frac{dU}{dI} = -Z_L\,. \tag{17}$$

The derivative in Eq. (15) can be calculated by $dI/dW=(dI/dT)(dT/dW)$ where dI/dT is given by Eq. (14)

while dT/dW is obtained by differentiation of Eq. (5) and can be approximated by $dT/dW=1/(A–dP_{T0}/dT)$ assuming again a negligible dA. The subtrahend in the bracket term corresponds to the feedback thermal conductance

$$G_F = -\frac{dP_{T0}}{dT}, \tag{18}$$

which is used to introduce the effective thermal admittance $A_{eff}=A+G_F$. Thus, the TB current responsivity formula finally reads

$$S_I = -\frac{\alpha_{TC} R_{TC} I + \gamma}{A_{eff}(R_{TC} + Z_L)}. \tag{19}$$

The TB voltage responsivity is calculated from Eq. (19) by means of Eq. (17). The effective thermal admittance can be expressed analogously to Eq. (6), i.e.

$$A_{eff}(\omega) = G_{eff} + i\omega C = G_{eff}(1 + i\omega\tau_{eff}) \tag{20}$$

where $\tau_{eff}=C/G_{eff}$ denotes the effective thermal time constant and

$$G_{eff} = G + G_F = G(1 + L_0) \tag{21}$$

is the effective thermal conductance. $L_0=G_F/G$ can be interpreted as a DC feedback gain. A negative feedback enhancing the thermal conductance, thus reducing responsivity and time constant, is associated with $L_0>0$. Eq. (19) can be rewritten by means of Eqs. (20) and (21). The TB current responsivity then reads

$$S_I = -\frac{\alpha_{TC} R_{TC} I + \gamma}{G(1 + L_0)(R_{TC} + Z_L)(1 + i\omega\tau_{eff})}, \quad \tau_{eff} = \frac{\tau}{1 + L_0}. \tag{22}$$

The detailed calculation of L_0 is given in the Appendix A. Its result is

$$L_0 = L_{ETF} + L_{TEF} = -\Lambda_{ETF}\frac{R_{BO} + R_L}{R_{TC0} + R_L}\beta - \Lambda_{TEF}\left(1 - \frac{R_{TC0}\alpha_{TC0}T}{R_{TC0} + R_L}\right) \tag{23}$$

where L_{ETF} and L_{TEF} denote the electrothermal and the thermoelectric components, respectively, of the DC feedback gain while Λ_{ETF} and Λ_{TEF} are abbreviations, i.e. $\Lambda_{ETF}=\alpha_{TC0}R_{TC0}I_0^2/G=(\alpha_{TC0}R_{TC0}I_0)\cdot(I_0/G)$ and $\Lambda_{TEF}=\gamma(I_0/G)=Y_0$. Furthermore, $R_L=Z_{L0}$ and β represents the expression

$$\beta = \frac{R_L(1 - Y_0) - R_{TC0}}{R_L(1 - Y_0)^2 + R_{TC0}}. \tag{24}$$

If $R_L\to\infty$, i.e. in the constant current mode of operation, then $L_{ETF}=-\Lambda_{ETF}$ and $L_{TEF}=-\Lambda_{TEF}$. The DC value of the thermocouple effective resistance, cf. Eq. (9), is given by $R_{TC0}=R_{BO}+R_D$ where $R_D=Z_{D0}$ is its DC dynamic resistance. Introducing the dimensionless figure of merit of a thermocouple

$$M_{TC} = \frac{R_D}{R_{BO}} = \frac{\gamma^2 T}{R_{BO} G} \tag{25}$$

R_{TC0} can be rewritten as

$$R_{TC0} = R_{BO}(1 + M_{TC}). \tag{26}$$

The DC value of the TB current responsivity S_{I0} is obtained from Eq. (22) to be

$$S_{I0} = -\frac{\alpha_{TC0} R_{TC0} I_0 + \gamma}{G \cdot r}, \quad r = (1 + L_0)(R_{TC0} + R_L). \tag{27}$$

Using the above definitions of Λ_{ETF} and Λ_{TEF} and Eq. (23) we get

$$S_{I0} = -\frac{\Lambda_{ETF} + \Lambda_{TEF}}{I_0\left[R_{TC0} + R_L - \Lambda_{ETF}(R_{BO} + R_L)\beta - \Lambda_{TEF}(R_{TC0} + R_L - R_{TC0}\alpha_{TC0}T)\right]} \tag{28}$$

from Eq. (27). If $R_L\to 0$, i.e. in the constant voltage mode of operation, and for small γ and α_{TC0}, i.e. if $Y_0(\gamma)<<1$, $R_D<<R_{BO}$ equivalent to $M_{TC}(\gamma)<<1$ as well as $\alpha_{TC0}T<<1$, then Eq. (28) simplifies to

$$S_{I0} = -\frac{1}{I_0 R_{TC0}} \frac{\Lambda_{ETF}(1+X)}{1+\Lambda_{ETF}(1-X)}, \quad X = \frac{\Lambda_{TEF}}{\Lambda_{ETF}}, \tag{29}$$

which corresponds to the DC part of a related equation given by Kaila and Russell [6].

Let us now consider two limiting cases of Eq. (28) in their consequences regarding the DC voltage responsivity of the TB, which is calculated by the relation $S_{U0}=-R_L S_{I0}$ from Eq. (28). The first one is the case of the conventional RB associated with $\gamma=0$ while the second one is the case of the unbiased thermocouple associated with $I=0$. In the first limiting case we get

$$S_{U0} = \frac{\Lambda B}{I_0(1-\Lambda\beta)}, \quad B = \frac{R_L}{R_L+R_{BO}}, \quad \beta = \frac{R_L-R_{BO}}{R_L+R_{BO}} \tag{30}$$

where $\Lambda=\alpha_{BO}P_{BO}/G$ is the bolometer DC electrothermal feedback gain in the constant voltage mode and B denotes the bridge factor. Eq. (30) corresponds to the results of the theory of the bolometer by Smith et al. (cf. §3.3.1 in [4]). For $R_L\to\infty$ $B=\beta=1$ is obtained and, thus, $S_{U0}=(1/I_0)\cdot\Lambda/(1-\Lambda)$, which complies with the results of de Nivelle *et al* (cf. Eq. (4) in [7]). In the second limiting case

$$S_{U0} = \frac{\gamma}{G}\frac{R_L}{R_{BO}+R_D+R_L} \tag{31}$$

is obtained. For $R_L\to\infty$ Eq. (31) is simplified to the known formula of the open circuit DC thermocouple voltage responsivity $S_{U0}=\gamma/G$ (cf. §3.2.2 in [4]).

4. Detectivity of the thermocouple bolometer

The specific detectivity of a radiation sensor (referred to as detectivity for brevity throughout this paper) is defined by

$$D^* = \varepsilon\frac{\sqrt{F}}{NEP} \tag{32}$$

where F is its receiver area and NEP denotes the noise equivalent power per square root bandwidth (NEP), which gives $\mathrm{cmHz^{1/2}/W}$ as the measuring unit of D^*. Note that the optical NEP is given by NEP/ε, which means that, with respect to NEP, the ideal case $\varepsilon=1$ is assumed. Three main noise components are considered in bolometers: temperature fluctuation noise (also termed phonon or thermal noise) represented by NEP_T, Johnson noise (NEP_J) and $1/f$ noise (NEP_F). For the total NEP the relation

$$NEP^2 = NEP_T^2 + NEP_J^2 + NEP_F^2 \tag{33}$$

holds true if the noise contributions are independent. The components are given by

$$NEP_T^2 = 4k_B T^2 G, \tag{34}$$

$$NEP_J^2 = 4k_B T P_{BO}\left|\frac{1+i\omega\tau}{\Lambda}\right|^2, \tag{35}$$

$$NEP_F^2 = \frac{2\pi}{\omega}c_F P_{BO}^2\left|\frac{1+i\omega\tau}{\Lambda}\right|^2 \tag{36}$$

[5, 7] where k_B denotes Boltzmann's constant, $c_F=\eta_H/(n_c V_R)$, η_H is the Hooge parameter [8], n_c the charge carrier density and V_R the volume of the resistor. A correction factor due to the temperature dependence of the thermal conductance as introduced by Mather in the expression of the phonon noise [5] is not taken into account, i.e. set to unity, in Eq. (34), which is justified for small temperature gradients. Dividing Eq. (35) by Eq. (34) we get $(NEP_J/NEP_T)^2=(1+\omega^2\tau^2)/M_{BO}$ for the bolometer where

$$M_{BO} = \Lambda\alpha_{BO}T = \frac{(\alpha_{BO}U_{BO})^2 T}{R_{BO}G}. \tag{37}$$

For the thermocouple, on the other hand, $(NEP_J/NEP_T)^2=(1+\omega^2\tau^2)/M_{TC}$ with M_{TC} given by Eq. (25) is valid (cf. §7.1 in [4]). Thus, analogously to the dimensionless figure of merit of a thermocouple, M_{BO} can be considered as the dimensionless figure of merit of a RB. On the other hand, Eq. (36) divided by Eq. (35) gives

$$NEP_F^{\,2}=\frac{s}{\omega}NEP_J^{\,2},\quad s=\frac{\pi}{2}\frac{c_F P_{BO}}{k_B T}. \tag{38}$$

Concerning the TB, Eq. (34) applies likewise. Eq. (38) is also assumed to remain valid. The bolometer DC electrothermal feedback gain $\Lambda=\alpha_{BO}P_{BO}/G$ can be expressed as $\Lambda=-I_0S_{I0}r$ by applying Eq. (27) to a RB (i.e. at $\gamma=0$). Using this relation for the substitution of $|\Lambda|$ in Eq. (35) results in $NEP_J^2=4k_BTR_{BO}(1+\omega^2\tau^2)/(S_{I0}r)^2$. As an approximation this expression of the Johnson NEP deduced for RB will be also applied to TB employing $S_{I0}r=-(\alpha_{TC0}R_{TC0}I_0+\gamma)/G$ valid for a TB (cf. Eq. (27)) rather than $S_{I0}\cdot r=-\alpha_{BO}U_{BO}/G$ valid for a RB. Within this approximation, the Johnson noise component of the TB can finally be expressed by

$$NEP_J^{\,2}=\frac{4k_BTR_{BO}G^2}{(\alpha_{TC0}R_{TC0}I_0+\gamma)^2}(1+\omega^2\tau^2). \tag{39}$$

Dividing Eq. (39) by Eq. (34) results in

$$NEP_J^{\,2}=\frac{1+\omega^2\tau^2}{M}NEP_T^{\,2} \tag{40}$$

where

$$M=\frac{(\alpha_{TC0}R_{TC0}I_0+\gamma)^2T}{R_{BO}G} \tag{41}$$

is the dimensionless figure of merit of a TB. Concerning the limiting cases Eq. (41) reduces to $M=M_{BO}$ if $\gamma=0$ and $M=M_{TC}$ if $I=0$, respectively. Starting from Eq. (33) and applying Eqs. (34), (38) and (40) the total NEP of a TB can be written as

$$NEP=NEP_T\sqrt{1+\frac{1+\omega^2\tau^2}{M}\left(1+\frac{s}{\omega}\right)} \tag{42}$$

with M given by Eq. (41). By calculating the derivative of the total NEP with respect to ω from Eq. (42) the optimum angular frequency ω_{opt} yielding the minimum NEP or the maximum detectivity, respectively, can be deduced from the cubic equation $2\omega_{opt}^3+s\omega_{opt}^2-s/\tau^2=0$. Cardano's formula yields

$$\omega_{opt}=\sqrt[3]{-q+\sqrt{q^2+p^3}}+\sqrt[3]{-q-\sqrt{q^2+p^3}}-\frac{s}{6},\quad q=\frac{s^3}{216}-\frac{s}{4\tau^2},\quad p=-\frac{s^2}{36}. \tag{43}$$

If the $1/f$ noise is negligible, i.e. $s\to0$, then the DC operation ($\omega_{opt}=0$) gives the highest detectivity, as expected. Using Eqs. (32), (34) and (42) the detectivity of a TB finally reads

$$D^*=\frac{\varepsilon}{2T}\sqrt{\frac{F}{k_BG\left[1+\frac{1+\omega^2\tau^2}{M}\left(1+\frac{s}{\omega}\right)\right]}}. \tag{44}$$

From Eq. (44) it is obvious that the electrical resistance R_{BO} as well as the thermal conductance G and capacitance C have to be evaluated for the calculation of D^*, which will be done in the next section.

5. Electrical resistance, thermal conductance and thermal capacitance calculation

To facilitate analytical modeling calculations a simple geometry is chosen essentially made up of a free-standing substrate strip stretching over an thermally insulating rectangular cavity and supporting the thermocouple n- and p-layers, cf. Fig. 2. The receiver area for this geometry is $F=wL$. The cavity edge is assumed to be at heat sink temperature T_S. The resistivity of the thermocouple layers ρ_m (m=n, p)

depends on the strip's average temperature T. Using $\Delta T=T-T_S$ instead of T we have

$$\rho_m(\Delta T) = \rho_{Sm}(1+\alpha_m \Delta T) \tag{45}$$

where ρ_{Sm} is the m-layer resistivity at heat sink temperature and α_m denotes its respective temperature coefficient. The respective m-layer electrical resistance is given by

$$R_m(\Delta T) = \rho_m(\Delta T)\frac{l_m}{wd_m} \tag{46}$$

where $l_n=l$, $l_p=L-l$ and d_m is the m-layer thickness. Since $R_{BO}(\Delta T)=R_n(\Delta T)+R_p(\Delta T)$, we find using Eqs. (45) and (46)

$$R_{BO}(\Delta T) = \frac{1}{w}\left(\frac{l_n\rho_{Sn}}{d_n}+\frac{l_p\rho_{Sp}}{d_p}\right)(1+\alpha\Delta T), \quad \alpha = \frac{R_{Sn}\alpha_n + R_{Sp}\alpha_p}{R_{Sn}+R_{Sp}} \tag{47}$$

where $R_{Sm}=R_m(0)$. The temperature coefficient of the resistance R_{BO}, given by $\alpha_{BO}=(1/R_{BO})dR_{BO}/dT$, yields $\alpha_{BO}(\Delta T)=\alpha/(1+\alpha\Delta T)$ from Eq. (47), hence $\alpha=\alpha_{BO}(0)$.

As to the thermal conductance of the TB strip one has to consider two components, which are the thermal conductance due to the strip in-plane thermal conductivity G_{Lm} and the thermal surface conductance G_{Mm} (m=n,p again refers to the m-strip). They are calculated by [9]

$$G_{Lm} = \frac{w}{l_m}(\kappa_m d_m + \kappa_s d_s) \tag{48}$$

where κ_m and κ_s are the m-layer and the substrate thermal conductivities, respectively, and d_s is the substrate thickness and

$$G_{Mm}(\Delta T) = wl_m[h + 4(\varepsilon_m+\varepsilon_s)\sigma_{SB}(T_S+\Delta T)^3]. \tag{49}$$

The first term in the square bracket of Eq. (49) represents the conductive or convective heat transfer quantified by the heat transfer coefficient h to the ambient while the second term represents the radiative heat transfer where ε_m and ε_s are the m-layer and the substrate absorptivities and σ_{SB} is the Stefan-Boltzmann constant. The thermal conductance is proportional to the sum of these components,

$$G(\Delta T) = \xi\cdot[G_{Ln}+G_{Lp}+G_{Mn}(\Delta T)+G_{Mp}(\Delta T)]. \tag{50}$$

Here ξ is a bolometric correction factor. Its detailed calculation is explained in the Appendix B.

Eqs. (47) and (50) express the electrical resistance and the thermal conductance, respectively, as a function of ΔT, which is in turn a function of the bias voltage U_B. In the limit of negligible W

$$\Delta T = \frac{P_{T0}(\Delta T, U_B)}{G(\Delta T)} \tag{51}$$

is found from Eq. (5) at ω=0. Eq. (51) has to be solved self-consistently to determine $\Delta T=\Delta T(U_B)$. In this equation the DC value P_{T0} of the total non-radiation induced heat load is given by

$$P_{T0}(\Delta T, U_B) = \gamma\cdot(T_S+\Delta T)I_0(\Delta T, U_B) + [U_B - R_L I_0(\Delta T, U_B)]I_0(\Delta T, U_B) \tag{52}$$

where

$$I_0(\Delta T, U_B) = \frac{U_B - \gamma\Delta T}{R_{BO}(\Delta T)+R_L} \tag{53}$$

in accordance with Eq. (11). Finally, the thermal capacitance is calculated by

$$C = c_{Vn}V_n + c_{Vp}V_p + c_{Vs}V_s \tag{54}$$

where c_{Vm} and c_{Vs} are the m-layer and the substrate volumetric heat capacities and $V_m=l_m w d_m$ and $V_s=Lwd_s$ are the respective volumes.

6. Modeling results and discussion

Bismuth (n-type) and antimony (p-type) have been shown to be a well-suited thermoelectric materials combination for high detectivity thin film radiation thermopiles [10]. Suitable alloying with Sb increases

the absolute Seebeck coefficient of thin Bi films by up to about 50%, with the optimum at x=0.13 for a $Bi_{1-x}Sb_x$ film [11]. On this basis, n-$Bi_{0.87}Sb_{0.13}$ and p-Sb thin films are chosen here as thermocouple legs for the TB to be modeled as an example. The junction of the BiSb/Sb thermocouple formed by these films is assumed to have an ohmic contact with a negligible contact resistance. The parameters used for the calculation of its responsivity and detectivity are listed in Table 2. For comparison a $Bi_{0.87}Sb_{0.13}$ thin film RB will be modeled, whose parameters are identical to the greatest extend with those of the related TB. Only the p-indexed parameter values of the TB labeled with an asterisk in Table 2 have to be replaced by their respective n-indexed values to switch from the TB to the related RB. Both the TB and the RB have a micro-bridge structure with a length of 30 µm and a width of 1.5 µm. Moreover, a high load resistance $R_L=100R_{BO}(0)$ in the bias circuit is chosen in both cases. The order of magnitude of the Hooge parameter was estimated from measurements of the noise power spectrum of thin Bi films (L=120 µm, w=10 µm, d=0.1 µm) made by Voss and Clarke [12].

An overview of the modeling results in the special case of an unbiased TB/RB ($I_0=0$) is given in Table 3. The results in the general case ($I_0\neq0$) are shown in Figs. 3 to 9. The dependence of the average temperature difference on the DC bias current deduced from Eq. (51) to (53) is presented in Fig. 3. I_0 was limited in both directions so that the resulting average temperature difference did not exceed ΔT_{max}=20 K. Contrary to the RB the curve referring to the TB is not symmetric with respect to $I_0=0$ due to the Peltier effect. This effect also causes the cooling at negative values of I_0, cf. Eq. (1), where Peltier cooling competes with Joule heating, thus leading to a minimum ΔT_{min}=–0.95 K at I_0=–0.1 mA.

For comparison of the bias-dependent properties of different bolometers, e.g., a TB with a RB or of bolometers of different size and resistance, it is advisable to refer to bias-induced average temperature differences as done in Figs. 4 to 9. Fig. 4 showing the absolute value of the DC voltage responsivity illustrates the different bias-induced behavior of the TB compared with the RB. As a matter of course, the RB has a vanishing responsivity at zero bias (ΔT=0), whereas the responsivity of the TB vanishes at ΔT=6.8 K corresponding to a bias current of about +0.18 mA. The bias current I_v related to a vanishing DC responsivity is calculated from Eq. (27) to be $I_v=-\gamma/(\alpha_{TC0}R_{TC0})$. Since γ as well as R_{TC0} are always positive a negative α_{TC0} results in a positive bias current I_v flowing from p to n through the thermocouple p-n junction. From Eq. (27) it can also be deduced that a biased TB will exhibit an improved responsivity compared to an unbiased TB if the current has the same sign as the temperature coefficient α_{TC0}. In the modeled example a negative bias current is necessary in this case, corresponding to the upper branch of the TB curve in Fig. 4 running from $|S_{U0}|$=63 V/W at ΔT=0, cf. Table 3, to $|S_{U0}|$=96 V/W at ΔT_{min} to $|S_{U0}|$=234 V/W at ΔT=20 K.

The bias-dependent behavior of the detectivity D^* calculated from Eq. (44) is presented at two different values of the angular frequency, 1 rad/s (low frequency mode) and ω_{opt} (high frequency mode), in Figs. 5 to 6 where the optimum angular frequency calculated from Eq. (43) is also bias-dependent as shown in Fig. 7. A value of 2980 rad/s is found for the optimum angular frequency at ΔT_{min}=–0.95 K corresponding to $D^*=3.0\times10^7$ cmHz$^{1/2}$/W while ω_{opt}=8990 rad/s at ΔT_{max}=20 K corresponding to $D^*=7.1\times10^7$ cmHz$^{1/2}$/W. The shape of the D^* curves is determined by the interplay described by Eq. (33) between the three NEP components NEP_T, cf. Eq. (34), NEP_J, cf. Eq. (40), and NEP_F, cf. Eq. (38). These components and the resulting total NEP of the TB are presented at the above-mentioned angular frequencies in Figs. 8 and 9. From these figures it can be stated with regard to the modeled TB that the temperature fluctuation noise (NEP_T) can be neglected at all frequencies including the optimum case depicted in Fig. 9. It is rather the Johnson noise (NEP_J) that is prevailing at ω_{opt}. A decrease of the angular frequency, however, brings the 1/f noise (NEP_F) more and more into play, which is finally dominating the overall NEP, cf. Fig. 8, with the exception of the interval representing a bias current close to zero where NEP_J is still dominant. Table 4 summarizes the results as to an advantageous TB operation extracted from the modeling results. The lowest NEP value concerning the biased BiSb/Sb thermocouple considered here is 9.5 pW/Hz$^{1/2}$ at optimum angular frequency and bias ΔT_{max}=20 K (cf. Fig. 9). This compares with the measured value of 13.1 pW/Hz$^{1/2}$ of an unbiased NiFe/Cr air-bridge

thermocouple of a similar strip geometry (L=75 µm, w=1 µm) recently published by Cox et al. [13]. As a theoretical lower bound, a background limited (BLIP) thermal sensor with a receiver area of 75 (µm)² would show a NEP of 0.048 pW/Hz$^{1/2}$ at 300 K.

Let us now compare the TB with the RB regarding the bias-dependent detectivity as illustrated in Figs. 5 and 6. In the low frequency range, cf. Fig. 5, it is obviously advantageous to operate the TB unbiased to avoid 1/f noise. Here the detectivity of the TB (2.33×10^7 cmHz$^{1/2}$/W, cf. Table 3) is one order of magnitude greater than the detectivity of the corresponding RB even at the maximum bias ΔT_{max}=20 K. Any biasing of the TB would decrease the detectivity at low frequencies. However, at optimum frequency, cf. Fig. 6, biasing by a negative current increases the detectivity of the TB, namely by a factor of 3 at ΔT_{max}=20 K. Here the detectivity of the RB is slightly higher compared with the TB only at ΔT>16.9 K.

7. Conclusion

Depending on the operational frequency, the thermocouple bolometer essentially being a biased radiation thermocouple can be advantageously operated in two basic operating modes to optimally control the influence of 1/f noise. In the low frequency mode it is operated unbiased to suppress 1/f noise dominating in this frequency range. In the high frequency mode where 1/f noise is exceeded by Johnson noise it is operated using a bias current of the same sign as its temperature coefficient of resistance α_{TC0}, thus improving considerably its detectivity in comparison to the unbiased operation. In this way of operation, the thermocouple bolometer combines the known advantage of a radiation thermocouple over a resistance bolometer, namely its unbiased and, hence, 1/f noise-free operation, with the resistance bolometer characteristic to increase its responsivity and detectivity by raising the bias current. In the example considered here, a detectivity improvement by a factor of 3 was calculated in the high frequency mode at a bias-induced temperature difference of 20 K, but there is potential for further improvements by choosing appropriate thermocouple materials with large temperature coefficients of resistance in addition to a high thermoelectric figure of merit.

Appendix A

The derivative in Eq. (18) for the calculation of feedback thermal conductance G_F can be rewritten as

$$\frac{dP_{T0}}{dT} = \alpha_{TC0} R_{TC0} \frac{dP_{T0}}{dR_{TC0}}. \tag{A.1}$$

Since $P_{T0}=\gamma T I_0+P_0$ one gets

$$\frac{dP_{T0}}{dR_{TC0}} = \frac{dP_0}{dR_{TC0}} + \gamma \cdot \left(I_0 \frac{dT}{dR_{TC0}} + T \frac{dI_0}{dR_{TC0}} \right). \tag{A.2}$$

With

$$\frac{dI_0}{dR_{TC0}} = -\frac{I_0 + \frac{\gamma}{G}\frac{dP_0}{dR_{TC0}}}{R_{TC0} + R_L} \tag{A.3}$$

derived from the DC part of Eq. (12) assuming that dG is negligible, Eq. (A.2) is rewritten as

$$\frac{dP_{T0}}{dR_{TC0}} = \gamma I_0 \frac{dT}{dR_{TC0}} - \frac{\gamma T I_0}{R_{TC0} + R_L} + \frac{dP_0}{dR_{TC0}} \left(1 - \frac{R_D}{R_{TC0} + R_L} \right) \tag{A.4}$$

Here $R_L=Z_{L0}$ is the load resistance. From $P_0= R_0 I_0^2$ follows

$$\frac{dP_0}{dR_{TC0}} = I_0^2 \left(\frac{dR_0}{dR_{TC0}} + 2\frac{R_0}{I_0}\frac{dI_0}{dR_{TC0}} \right). \tag{A.5}$$

The relation between R_{TC0} and R_0 is

$$R_0 = \frac{R_{TC0}}{1-Y_0} \tag{A.6}$$

with $Y_0=\gamma I_0/G$ obtained from Eq. (10) at ω=0. Assuming again that dG is negligible differentiation of Eq. (A.6) yields

$$\frac{dR_0}{dR_{TC0}} = \frac{1+R_0\dfrac{Y_0}{I_0}\dfrac{dI_0}{dR_{TC0}}}{1-Y_0}. \tag{A.7}$$

Using Eqs. (A.6) and (A.7) to transform Eq. (A.5) dP_0/dR_{TC0} is found to be

$$\frac{dP_0}{dR_{TC0}} = \frac{{I_0}^2}{1-Y_0}\left[1+\frac{2-Y_0}{1-Y_0}\frac{R_{TC0}}{I_0}\frac{dI_0}{dR_{TC0}}\right]. \tag{A.8}$$

Again using Eq. (A.3) to rewrite Eq. (A.8) finally yields

$$\frac{dP_0}{dR_{TC0}} = {I_0}^2\beta, \quad \beta = \frac{R_L(1-Y_0)-R_{TC0}}{R_L(1-Y_0)^2+R_{TC0}}. \tag{A.9}$$

Now the DC feedback gain $L_0=G_F/G=-(1/G)\cdot dP_{T0}/dT$ can be calculated from Eqs. (A.1), (A.4) and (A.9) resulting in

$$L_0 = -\frac{{I_0}^2 R_{TC0}\alpha_{TC0}(R_{BO}+R_L)\beta+\gamma I_0\left[R_{TC0}(1-\alpha_{TC0}T)+R_L\right]}{G(R_{TC0}+R_L)}, \tag{A.10}$$

which is rewritten to form Eq. (23).

Appendix B

The bolometric correction factor ξ is calculated as the zero bias limit (U_B =0) of the bias-dependent correction factor $\xi_U(U_B)$ by considering a RB, i.e. γ=0, and additionally excluding irradiation, i.e. W=0. In this case the thermal conductance G can be expressed by $P_{BO}/\Delta T$. Applying this relation and solving Eq. (50) for $\xi_U(U_B)$ we get

$$\xi_U(U_B) = \frac{\dfrac{P_{BO}(\Delta T(U_B),U_B)}{\Delta T(U_B)}}{G_{Ln}+G_{Lp}+G_{Mn}(\Delta T(U_B))+G_{Mp}(\Delta T(U_B))} \tag{B.1}$$

where

$$P_{BO}(\Delta T,U_B) = \left(\frac{U_B}{R_{BO}(\Delta T)+R_L}\right)^2 R_{BO}(\Delta T) \tag{B.2}$$

and finally the bolometric correction factor

$$\xi = \xi_U(0). \tag{B.3}$$

Hence, $\Delta T(U_B)$ has to be calculated to determine ξ, which can be accomplished by modeling the stationary temperature distribution in the bolometer strip based on the geometry shown in Fig. 2. For this purpose the one-dimensional heat transport equation

$$\frac{d^2}{dx^2}\delta T_m(x) - \left(\frac{\nu_m}{l_m}\right)^2\left(\delta T_m(x)-T_{Mm}\right) = 0, \quad m = \mathrm{n,p} \tag{B.4}$$

has to be solved [9]. Here $\delta T_m(x)$ is the deviation of temperature distribution along the strip from the heat sink temperature, ${\nu_m}^2$ is the thermal conductance ratio

$${\nu_m(\Delta T)}^2 = \frac{G_{Mm}(\Delta T)}{G_{Lm}} \tag{B.5}$$

and

$$T_{Mm}(\Delta T, U_B) = \left(\frac{U_B}{R_{BO}(\Delta T) + R_L} \right)^2 \frac{R_m(\Delta T)}{G_{Mm}(\Delta T)} . \quad \text{(B.6)}$$

Applying the boundary conditions $\delta T_m(0)=0$ and $\delta T_m(l_m)=\theta$ the solution is [9]

$$\delta T_m(x,\theta) = [\theta - T_{Mm}(1-\cosh(\nu_m))] \frac{\sinh\left(\frac{\nu_m}{l_m} x\right)}{\sinh(\nu_m)} + T_{Mm}\left(1-\cosh\left(\frac{\nu_m}{l_m} x\right)\right) \quad \text{(B.7)}$$

where θ denotes the temperature difference between the hot junction and the heat sink. θ can be determined by the condition of heat flow continuity at $x=l$, which reads

$$\sum_m l_m G_{Lm} \frac{d}{dx} \delta T_m(x,\theta) = 0 . \quad \text{(B.8)}$$

The result is

$$\theta = \frac{\sum_m G_{Lm} \nu_m T_{Mm} \tanh\left(\frac{\nu_m}{2}\right)}{\sum_m G_{Lm} \nu_m \coth(\nu_m)} . \quad \text{(B.9)}$$

Eq. (B.7) with θ substituted by Eq. (B.9) shows that $\delta T_m = \delta T_m(x, \Delta T(U_B), U_B)$ where the dependence on $\Delta T(U_B)$ and U_B arises from the quantities given by Eqs. (B.5) and (B.6). Finally, by integration over the spatial coordinate x, the mean temperature difference of the bolometer strip to the heat sink ΔT is calculated to be

$$\Delta T(U_B) = \frac{1}{L} \left(\int_0^l \delta T_n(x, \Delta T(U_B), U_B) dx + \int_l^L \delta T_p(L-x, \Delta T(U_B), U_B) dx \right). \quad \text{(B.10)}$$

This integral equation has to be solved self-consistently for $\Delta T(U_B)$. Then, with the result inserted in Eqs. (B.1) and (B.2), the bolometric correction factor can be calculated using Eq. (B.3).

Acknowledgment

This work was funded by the Bundesministerium für Bildung und Forschung, project TeraCam, Grant No. 13N9304.

References

[1] van Herwaarden A W and van Oudheusden B 1994 *Thermal sensors* ed G C M Meijer and A W van Herwaarden (Bristol and Philadelphia: Institute of Physics Publishing) chapter 1
[2] Conn G K T 1945 *Trans. Faraday Soc.* **41** (1945) 192
[3] Jones R C 1953 *J. Opt. Soc. Am.* **43** 1
[4] Smith R A, Jones F E and Chasmar R P 1968 *The detection and measurement of infra-red radiation* (Oxford: Clarendon Press)
[5] Mather J C 1982 *Appl. Opt.* **21** 1125
[6] Kaila M M and Russell G J 2000 *J. Supercond.* **13** 1025
[7] de Nivelle M J M E *et al* 1997 *J. Appl. Phys.* **82** 4719
[8] Hooge F N, Kleinpenning T G M and Vandamme L K J 1981 *Rep. Prog. Phys.* **44** 479
[9] Dillner U 1994 *Sensors and Actuators A* **41-42** 260
[10] Völklein F and Wiegand A 1990 *Sensors and Actuators A* **24** 1
[11] Völklein F and Kessler E 1987 *Thin Solid Films* **155** 197
[12] Voss R F and Clarke J 1976 *Phys. Rev. B* **13** 556

[13] Cox J A, Higashi R, Nusseibeh F, Newstrom-Peitso K, Zins C, Osiander R, Lehtonen J and Dodson E, *Proc. SPIE* **7311** (2009) 73110R-1
[14] Völklein F and Kessler E 1990 *Phys. Stat. Sol. (b)* **158** 521
[15] Völklein F and Kessler E 1987 *Phys. Stat. Sol. (b)* **143** 121
[16] Völklein F and Dillner U 1990 *Phys. Stat. Sol. (b)* **162** 147

Captions

Table 1. Formulae of the resistance, the voltage drop and Joule heating power of a TB compared with a RB.

Table 2. Parameters used for modeling the responsivity and detectivity of a $Bi_{0.87}Sb_{0.13}$/Sb thin film TB and a $Bi_{0.87}Sb_{0.13}$ thin film RB, respectively. The p-indexed parameter values labeled with an asterisk (*) have to be replaced by their respective n-indexed values for the RB modeling.

Table 3. Overview of modeling results at zero bias.

Table 4. TB operating modes and biasing recommendations.

Figure 1. TB bias circuit. U_B: bias voltage, I: bias current, R: TB resistance, U_{TE}: thermocouple thermoelectric e.m.f., R_{BO}: bolometer electrical resistance, Z_L: load impedance.

Figure 2. TB strip geometry. w: strip width, L: total length of the free-standing strip, l: n-strip length.

Figure 3. Bias-induced average temperature difference ΔT vs. DC bias current I_0 (TB: full curve, RB: dashed curve).

Figure 4. Absolute value of the DC voltage responsivity S_{U0} vs. bias-induced average temperature difference ΔT (TB: full curve, RB: dashed curve).

Figure 5. Detectivity D^* at an angular frequency of 1 rad/s vs. bias-induced average temperature difference ΔT (TB: full curve, RB: dashed curve).

Figure 6. Detectivity D^* at optimum angular frequency vs. bias-induced average temperature difference ΔT (TB: full curve, RB: dashed curve).

Figure 7. Optimum angular frequency ω_{opt} vs. bias-induced average temperature difference ΔT (TB: full curve, RB: dashed curve).

Figure 8. NEP and its components of the TB at an angular frequency of 1 rad/s vs. bias-induced average temperature difference ΔT .

Figure 9. NEP and its components of the TB at optimum angular frequency vs. bias-induced average temperature difference ΔT .

Table 1

Quantity	RB	TB
resistance	R_{BO}	$R = R_{BO}+Z_{TE} = R_{BO}+U_{TE}/I$
voltage drop	$U_{BO} = R_{BO}I$	$U = RI = U_{BO}+U_{TE}$
Joule heating power	$P_{BO} = U_{BO}I$	$P = UI = P_{BO}+U_{TE}I$

Table 2

Parameter	index: *n*	index: *p*	index: *s*
γ(μV/K)	–100 [11]	+35* [14]	-
ρ_S (μΩm)	7 [11]	1* [14]	-
α(%/K)	–0.45 [11]	+0.18* [14]	-
κ(W/(m·K))	3 [15]	13* [14]	1
ε	1	1	1
c_V (10^6 Ws/(m^3·K))	1.7	1.7	1.7
l (μm)	15	15	-
d (μm)	0.4	0.4	1
w (μm)	1.5		
n_c (10^{24}/m^3)	3 [16]		
η_H	10^{-5} [12]		
h (W/(m^2·K))	0 (vacuum)		
T_S (K)	300		

Table 3

quantity at I_0=0	TB	RB
α(%/K)	–0.371	–0.45
R_{BO} (Ω)	200	350
R_{TC0} (Ω)	202.6	350
G (μW/K)	2.12	1.32
τ(μs)	50.5	81.1
S_{U0} (V/W)	63.0	0
D_0* (10^7 cmHz$^{1/2}$/W)	2.33	0

Table 4

TB operating mode	Prevailing noise	Recommended TB biasing	Resulting advantage
low frequency mode	1/*f* noise	unbiased	no 1/*f* noise
high frequency mode	Johnson noise	same sign of bias current and temperature coefficient of resistance	enhanced responsivity and detectivity

Fig. 1

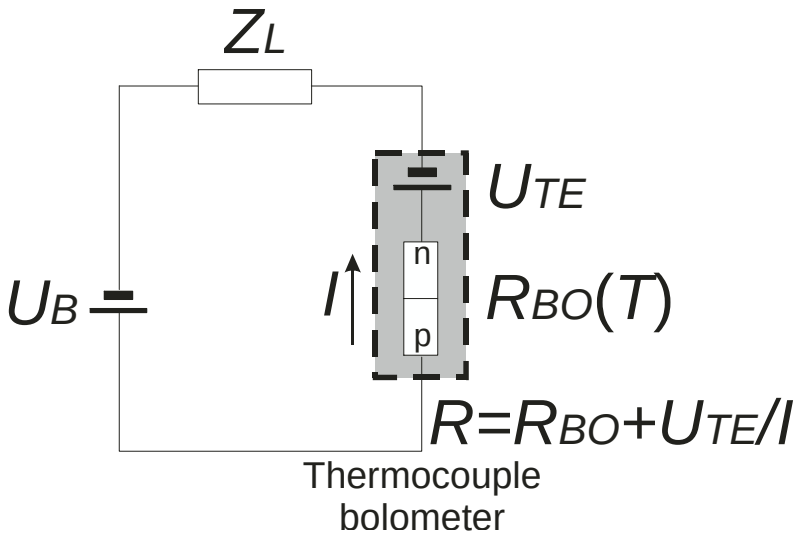
Z_L
U_{TE}
n
p
U_B
I
$R_{BO}(T)$
$R=R_{BO}+U_{TE}/I$
Thermocouple
bolometer

Fig. 2

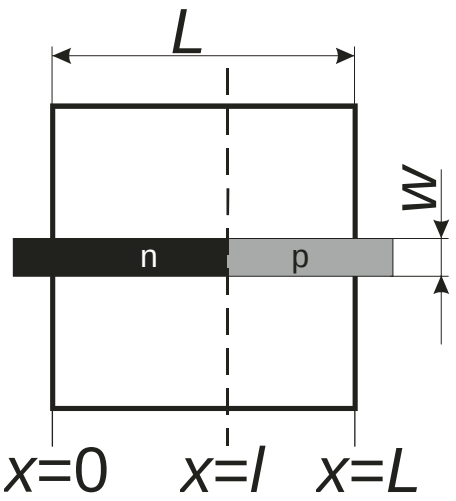
L
W
n
p
$x=0$
$x=l$
$x=L$

Fig. 3

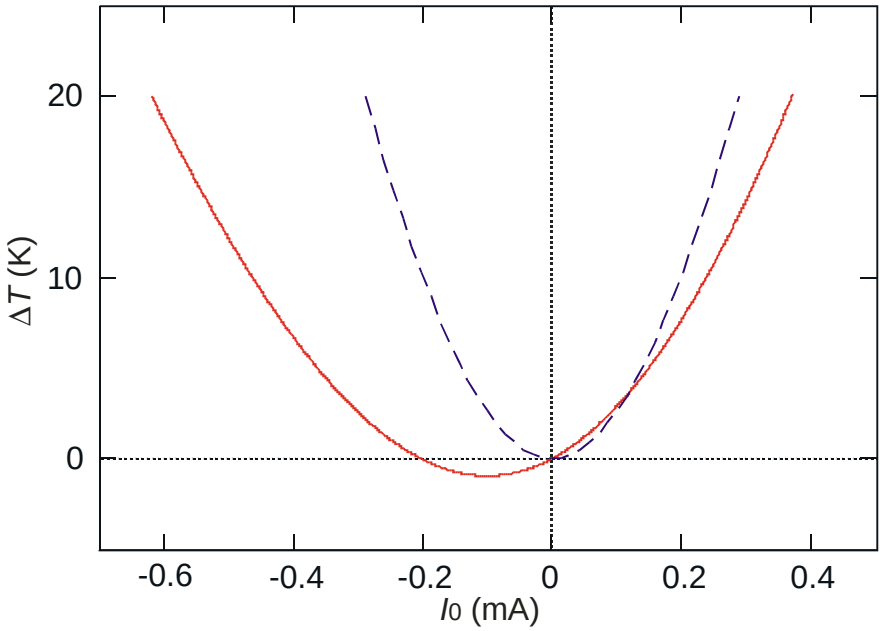
20
10
0
ΔT (K)
-0.6
-0.4
-0.2
0
0.2
0.4
I0 (mA)

Fig. 4

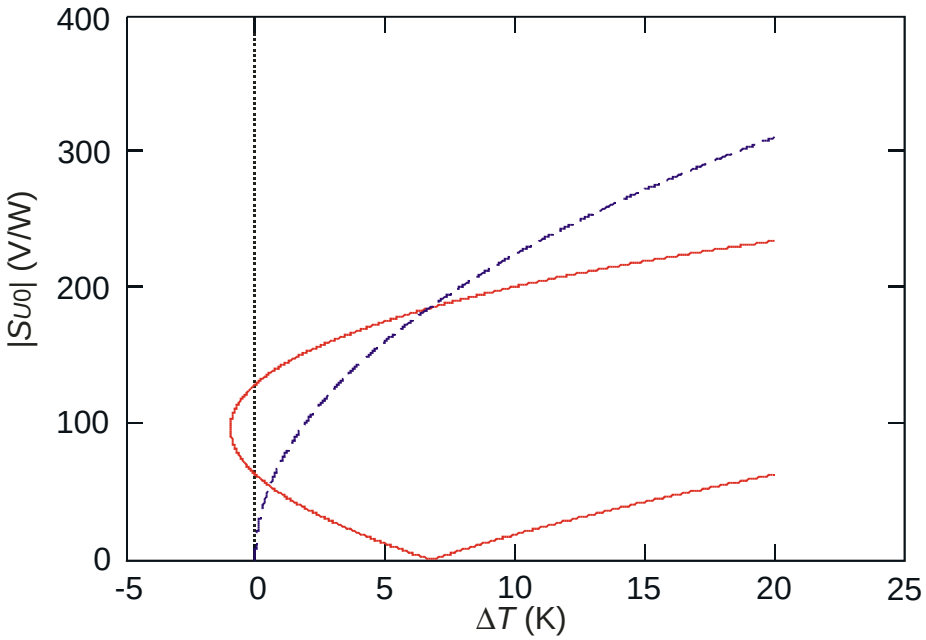
400
300
200
100
0
|SU0| (V/W)
-5
0
5
10
15
20
25
ΔT (K)

Fig. 5

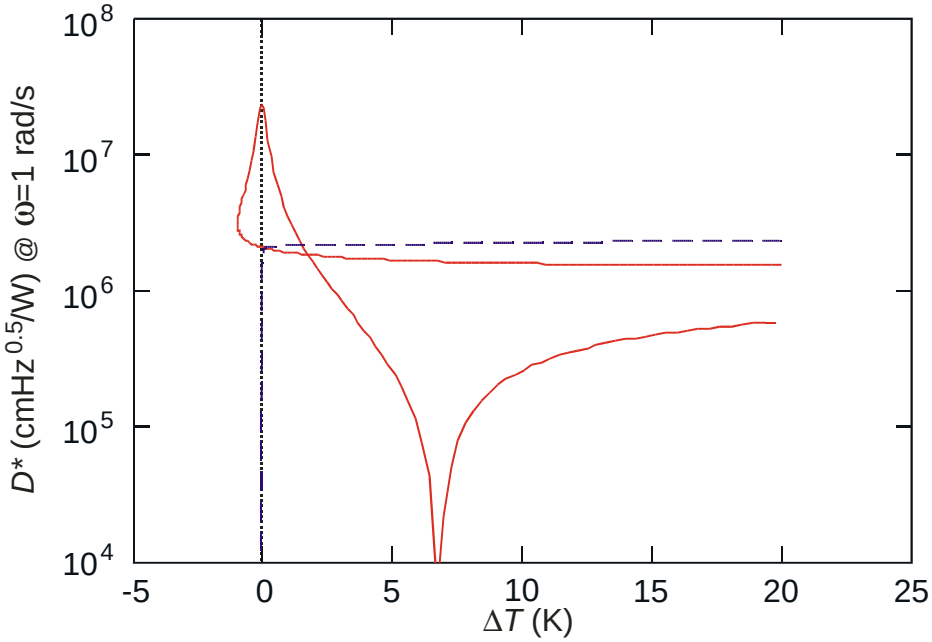
10^8
10^7
10^6
10^5
10^4
D^* (cmHz$^{0.5}$/W) @ ω=1 rad/s
-5
0
5
10
15
20
25
ΔT (K)

Fig. 6

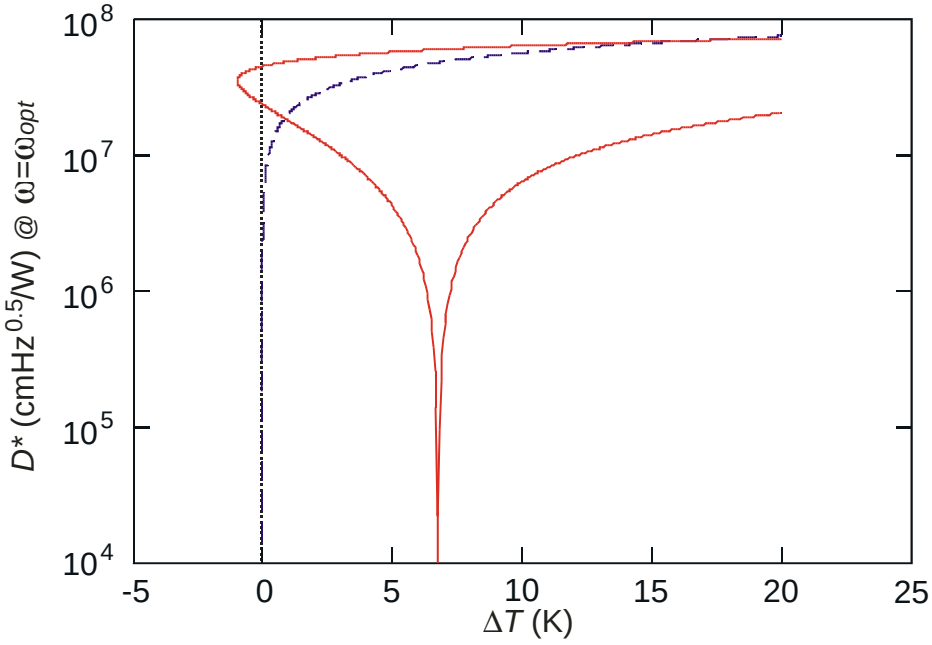
10^8
10^7
10^6
10^5
10^4
D^* (cmHz$^{0.5}$/W) @ ω=ω$_{opt}$
-5
0
5
10
15
20
25
ΔT (K)

Fig. 7

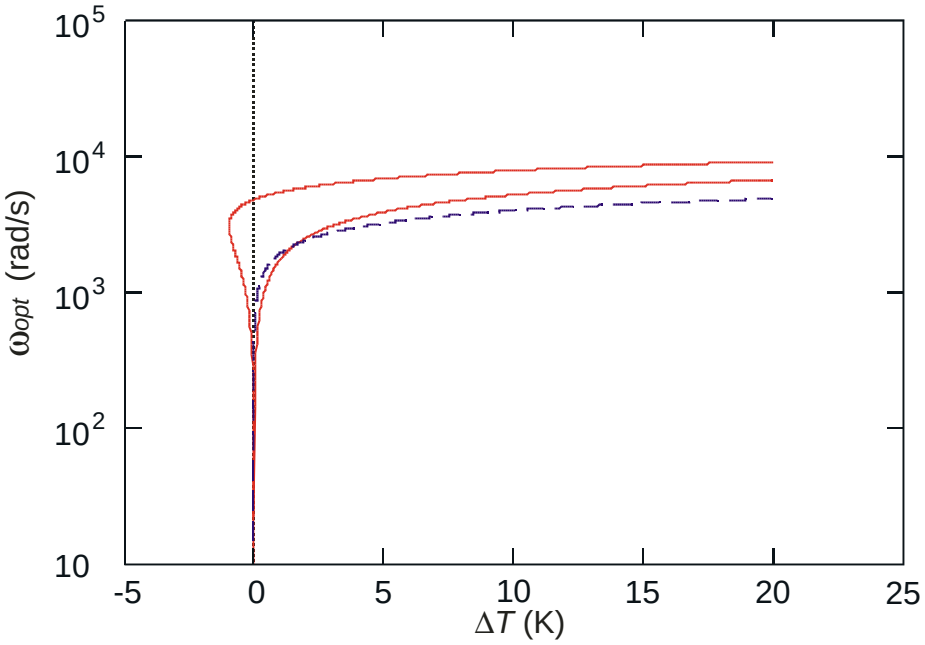
10^5
10^4
10^3
10^2
10
ω_{opt} (rad/s)
-5
0
5
10
15
20
25
ΔT (K)

Fig. 8

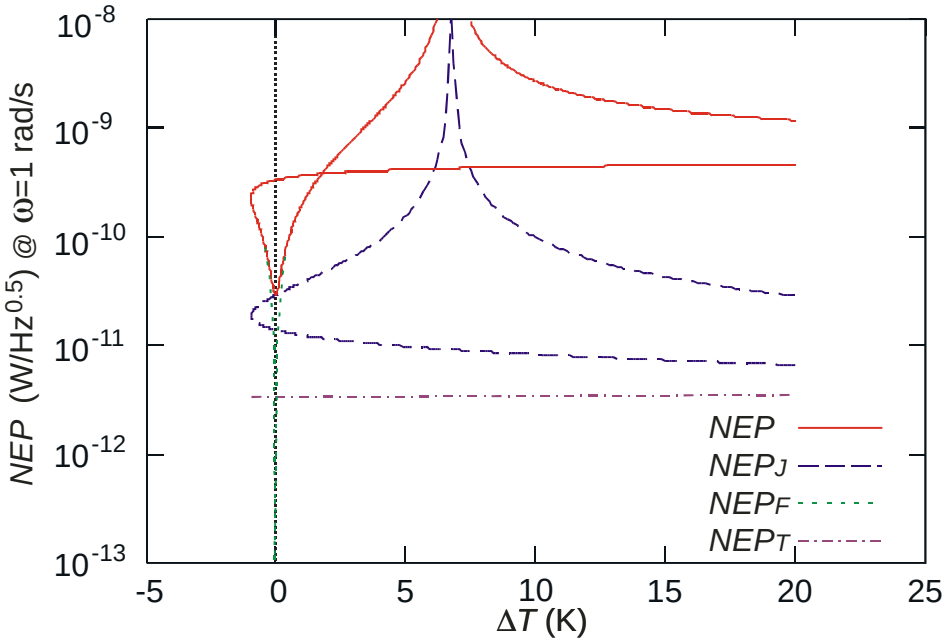
10^{-8}
10^{-9}
10^{-10}
10^{-11}
10^{-12}
10^{-13}
NEP (W/Hz$^{0.5}$) @ ω=1 rad/s
-5
0
5
10
15
20
25
ΔT (K)
NEP
NEP$_J$
NEP$_F$
NEP$_T$

Fig. 9

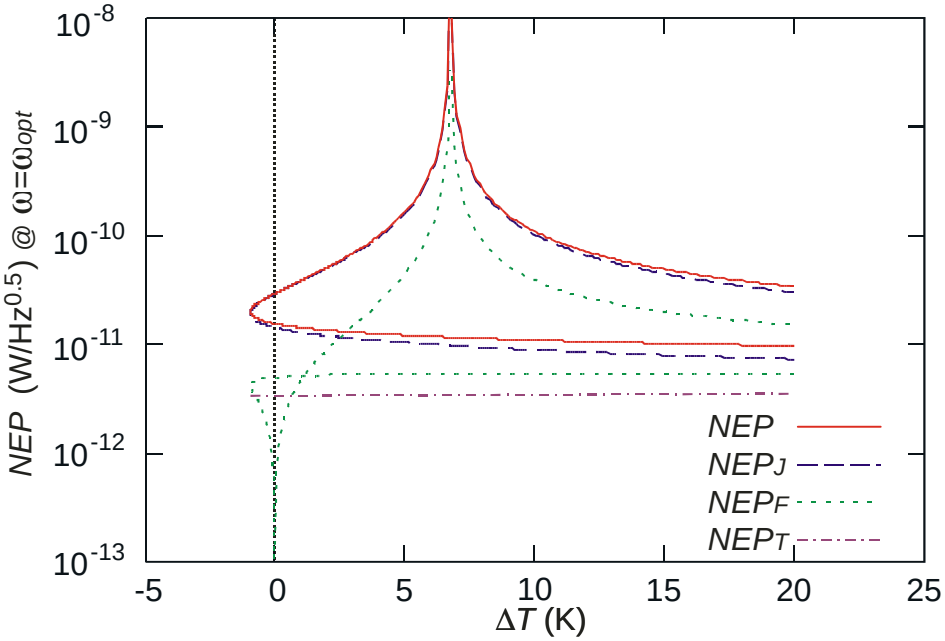
10-8
10-9
10-10
10-11
10-12
10-13
NEP (W/Hz0.5) @ ω=ωopt
-5
0
5
10
15
20
25
ΔT (K)
NEP
NEPJ
NEPF
NEPT